

Implicit integrations for smooth particle hydrodynamics in Semi-Lagrangian approach: application to the accretion disc modelling in a microquasar

G. Lanzafame*

INAF - Osservatorio Astrofisico di Catania, Via S. Sofia 78 - 95123 Catania, Italy

Accepted ——. Received ——; in original form ——

ABSTRACT

Current explicit integration techniques in fluid dynamics are deeply limited by the Courant-Friedrichs-Lewy condition of the time step progression, based on the adopted spatial resolution coupled with the maximum value between the kinetic velocity or the signal transmission speed in the computational domain. Eulerian implicit integration techniques, even though more time consuming, can allow to perform stable computational fluid dynamics even if such explicit limitation is very short, paying only the price of a very small inaccuracy in the calculations, without suffering such a strict (sometimes very strict) temporal limitation. In this paper, we present a simple and effective way to perform Free Lagrangian Smooth Particle Hydrodynamics (SPH) implicit integrations without any Jacobian matrix inversion operations. Applications to SPH accretion disc simulation around a massive black hole (MBH) in a binary stellar system is shown, together with a comparison to the same result obtained according to the traditional explicit integration techniques. A simple test in the case of an 1D blast wave is also discussed. Some necessary cautions in the SPH technique, never discussed before, to get the necessary convergence between the flow physics and its SPH mathematical counterpart, are also discussed.

Key words: accretion, accretion discs – conduction – convection – hydrodynamics: methods: numerical, N-body simulations – binaries: close – stars: novae, cataclysmic variables.

1 INTRODUCTION

A time step restriction is always necessary for time dependent calculations in computational fluid dynamics. Currently, such restrictions are needed for mathematical stability reasons in explicit calculations of partial differential equations (PDE), while they are necessary for accuracy considerations in implicit calculations. The integrated physical local property at time step level $n + 1$: A^{n+1} is a function of its previous values at time steps n , $n - 1$ etc., as well as of spatial derivatives of its spatial flux densities: $dF(A)/dr$, relative to the previous time steps for explicit calculations. Instead A^{n+1} is a function of these quantities also for the same $n + 1$ time step level for implicit calculations.

For computational flow explicit calculations, the Courant-Friedrichs-Lewy condition (Courant et al. 1928, 1967) is imposed on those hyperbolic terms representing advection in PDE (spatial derivatives of pressure or velocity),

where the given Courant number $C = v_c \Delta t / \Delta r \leq 1$ is generally of the order of 0.2 – 0.5, where Δr is the spatial resolution, v_c is the maximum value among the local kinematic and the signal transmission velocities within the computational domain, and Δt is the time step to be computed.

Explicit integration techniques are widely adopted to solve equations of the fluid dynamics both in the Eulerian formalism, where time and space derivatives refer both to local derivatives of the physical properties ($\partial/\partial t$ and $\partial/\partial r$), according to the adopted spatial resolution length, and in the Lagrangian formalism, where the material or the convective derivative $d/dt = \partial/\partial t + \mathbf{v} \cdot \nabla$ characterizes the flow description (Fletcher 1991; Hirsch 1997; LeVeque 2002). Implicit integration techniques are instead often applied to solve equations of the fluid dynamics only in the Eulerian formalism. In spite of such a dichotomy Ardeljan et al. (1996) produced an implicit Lagrangian method, based on a triangular grid for calculations of nonstationary astrophysical processes, whose results successfully compare with other Lagrangian explicit calculations, although some de-

* E-mail: glanzafame@oact.inaf.it

tails in the flow do not compare with those obtained via Eulerian formalism. Furthermore, Semi-Lagrangian schemes (Staniforth & Côté 1991) have been built up based on mixed explicit-implicit schemes, lengthening the time step up to a factor of 6, paying a little additional cost in the time computing, without any degradation in the accuracy of the solution (Robert 1969; Robert et al. 1972). However, such a maximum stable time step still remains much shorter than seems necessary from considerations of accuracy (Robert 1981).

Currently, SPH hydrodynamics works adopting an explicit integration technique, being SPH a "Free Lagrangian particle scheme" (Whitehurst 1995). Recently some authors (Whitehouse & Bate 2004; Susa 2006; Rook et al. 2007; Petkova & Springel 2009) developed implicit integration schemes working in SPH to solve some selected problems dealing with the radiative transfer or with the heat transfer in the flow, adopting either Crank-Nicolson, or the Runge-Kutta-Fehlberg integrator, or the conjugate gradient method. The adoption of such methods involves the handling of some time-expensive Jacobian matrices. Alternatively (Viau et al. 2006), some iterative variational techniques are also used to find zeros for the analytical equation coming out from the energy equation written in finite terms and including the diffusive terms, within an assigned tolerance error, setting the boundary "left" and "right" values for ϵ , finding the median value using the Van Wijngaarden-Dekker-Brent bisection method (Press et al. 1992). However, the introduction of such mixed procedures deviate from the original pure particle hydrodynamics.

For these reasons, in this paper we present a simple implicit mathematical technique able to perform implicit integrations both of the Euler and of the Navier-Stokes equations of the fluid dynamics, respecting the SPH, or the SPH-derived schemes, without any Jacobian matrix handling. Astrophysical applications are here presented on the study of an accretion disc around a MBH in a close binary system, both adopting the implicit and the explicit integration procedures. Some advantages are also discussed, compared to the explicit schemes, as well as a significant test is shown on the accuracy of the integration technique applied to SPH.

Successful applications are here reported for the case of a 1D blast wave case as well as for a full 3D astrophysical application to the accretion disc for a microquasar.

To conclude this paper, a refinement to SPH is also discussed in the appendix. The revision regards only the particle mass - mass density - numerical density correlations to get a full physical meaning of SPH interpolations. This caution is necessary whenever different mass SPH particles are considered.

2 FLUID DYNAMICS EQUATIONS AND THEIR SPH FORMULATION

The relevant equations to our model of viscous gas hydrodynamics are:

$$\frac{d\rho}{dt} + \rho \nabla \cdot \mathbf{v} = 0 \quad \text{continuity equation (1)}$$

$$\frac{d\mathbf{v}}{dt} = -\frac{\nabla p}{\rho} + [-2\boldsymbol{\omega} \times \mathbf{v} + \boldsymbol{\omega} \times (\boldsymbol{\omega} \times \mathbf{r}) - \nabla \Phi_{grav}] +$$

$$\frac{1}{\rho} \nabla \cdot \boldsymbol{\tau} \quad \text{Navier-Stokes momentum equation (2)}$$

$$\frac{d}{dt} \left(\epsilon + \frac{1}{2} v^2 \right) = -\frac{1}{\rho} \nabla \cdot (p\mathbf{v} - \mathbf{v} \cdot \boldsymbol{\tau}) + \mathbf{g} \cdot \mathbf{v} \quad \text{energy equation (3)}$$

$$p = f(\gamma, \rho, \epsilon, \mathbf{r}, \mathbf{v}) \quad \text{perfect gas equation (4)}$$

$$\frac{d\mathbf{r}}{dt} = \mathbf{v} \quad \text{kinematic equation (5)}$$

d/dt stands for the Lagrangian derivative, ρ is the gas density, ϵ is the thermal energy per unit mass, Φ_{grav} is the effective gravitational potential generated by the two stars and $\boldsymbol{\omega}$ is the angular velocity of the rotating reference frame, corresponding to the rotational period of the binary system, p is the ideal gas pressure, here generally expressed as a function of local properties, determined by its equation of state (EoS). The adiabatic index γ has the meaning of a numerical parameter whose value lies in the range between 1 and 5/3, in principle. $\boldsymbol{\tau}$ is the viscous stress tensor, whose presence modifies the Euler equations for a non viscous fluid dynamics in the viscous Navier-Stokes equations.

The SPH method is a Free Lagrangian scheme that discretizes the fluid into moving interacting and interpolating domains called "particles" (Monaghan 1985, 1992; Monaghan & Lattanzio 1985). All particles move according to pressure and body forces. The method makes use of a Kernel W useful to interpolate a physical quantity $A(\mathbf{r})$ related to a gas particle at position \mathbf{r} according to:

$$A(\mathbf{r}) = \int_D A(\mathbf{r}') W(\mathbf{r}, \mathbf{r}', h) d\mathbf{r}' \quad (6)$$

$W(\mathbf{r}, \mathbf{r}', h)$, the interpolation Kernel, is a continuous function - or two connecting continuous functions whose derivatives are continuous even at the connecting point - defined in the spatial range $2h$, whose limit for $h \rightarrow 0$ is the Dirac delta distribution function. All physical quantities are described as extensive properties smoothly distributed in space and computed by interpolation at \mathbf{r} . In SPH terms we write:

$$A_i = \sum_{j=1}^N \frac{A_j}{n_j} W(\mathbf{r}_i, \mathbf{r}_j, h) = \sum_{j=1}^N \frac{A_j}{n_j} W_{ij} \quad (7)$$

where the sum is extended to all particles included within the domain D , $n_j = \rho_j/m_j$ is the number density relative to the j th particle. $W(\mathbf{r}_i, \mathbf{r}_j, h) \leq 1$ is the adopted interpolation Kernel whose value is determined by the relative distance between particles i and j .

In SPH conversion of mathematical equations (eq. 1 to eq. 4) there are two principles embedded. Each SPH particle is an extended, spherically symmetric domain where any physical quantity f has a density profile $fW(\mathbf{r}_i, \mathbf{r}_j, h) \equiv fW(|\mathbf{r}_i - \mathbf{r}_j|, h) = fW(|\mathbf{r}_{ij}|, h)$. Besides, the fluid quantity f at the position of each SPH particle could be interpreted by filtering the particle data for $f(\mathbf{r})$ with a single windowing function whose width is h . So doing, fluid data are considered isotropically smoothed all around each particle along a length scale h . Therefore, according to these two concepts, the SPH value of the physical quantity f is both the overlapping of extended profiles of all particles and

the overlapping of the closest smooth density profiles of f . This means that the compactness of the Kernel shape gives the principal contribution to the interpolation summation to each particle by itself and by its closest neighbours. In both approaches the mass is globally conserved in so far as the total particle number is constant.

In SPH formalism, equations (2) and (3) take the form:

$$\frac{d\mathbf{v}_i}{dt} = -\sum_{j=1}^N m_j \left(\frac{p_i^*}{\rho_i^2} + \frac{p_j^*}{\rho_j^2} \right) \nabla_i W_{ij} + \mathbf{g}_i + \sum_{j=1}^N m_j \left(\frac{\eta_{vi}\boldsymbol{\sigma}_i}{\rho_i^2} + \frac{\eta_{vj}\boldsymbol{\sigma}_j}{\rho_j^2} \right) \cdot \nabla_i W_{ij} \quad (8)$$

$$\frac{d}{dt}E_i = -\sum_{j=1}^N m_j \left(\frac{p_i^*\mathbf{v}_i}{\rho_i^2} + \frac{p_j^*\mathbf{v}_j}{\rho_j^2} \right) \cdot \nabla_i W_{ij} + \mathbf{g}_i \cdot \mathbf{v}_i + \sum_{j=1}^N m_j \left(\eta_{vi} \frac{\boldsymbol{\sigma}_i \cdot \mathbf{v}_i}{\rho_i^2} + \eta_{vj} \frac{\boldsymbol{\sigma}_j \cdot \mathbf{v}_j}{\rho_j^2} \right) \cdot \nabla_i W_{ij} \quad (9)$$

where $\mathbf{g}_i = -2\boldsymbol{\omega} \times \mathbf{v}_i + \boldsymbol{\omega} \times (\boldsymbol{\omega} \times \mathbf{r}_i) - \nabla \Phi_{grav,i}$, $\mathbf{v}_{ij} = \mathbf{v}_i - \mathbf{v}_j$, m_j is the mass of j th particle and $p_i^* = p_i + \text{dissipation pressure term}$. $E_i = (\epsilon_i + \frac{1}{2}v_i^2)$. The viscous stress tensor $\tau_{\alpha\beta}$ includes the positive first and second viscosity coefficients η_v and ζ_v which are velocity independent and describe shear and tangential viscosity stresses (η_v), and compressibility stresses (ζ_v):

$$\tau_{\alpha\beta} = \eta_v \sigma_{\alpha\beta} + \zeta_v \nabla \cdot \mathbf{v} \quad (10)$$

where the shear

$$\sigma_{\alpha\beta} = \frac{\partial v_\alpha}{\partial x_\beta} + \frac{\partial v_\beta}{\partial x_\alpha} - \frac{2}{3} \delta_{\alpha\beta} \nabla \cdot \mathbf{v} \quad (11)$$

In these equations α and β are spatial indexes while tensors are written in bold characters. For the sake of simplicity we assume $\zeta_v = 0$, however our code allows us also different choices. Defining

$$V_{i\alpha\beta} = \sum_{j=1}^N \frac{m_j v_{ji\alpha}}{\rho_j} \frac{\partial W_{ij}}{\partial x_\beta} \quad (12)$$

as the SPH formulation of $\partial v_\alpha / \partial x_\beta$, the SPH equivalent of the shear is:

$$\sigma_{i\alpha\beta} = V_{i\alpha\beta} + V_{i\beta\alpha} - \frac{2}{3} \delta_{\alpha\beta} V_{i\gamma\gamma} \quad (13)$$

A full justification of this SPH formalism can be found in Flebbe et al. (1994a,b).

In this scheme the continuity equation takes the form:

$$\frac{d\rho_i}{dt} = \sum_{j=1}^N m_j \mathbf{v}_{ij} \cdot \nabla_i W_{ij} \quad (14)$$

or, as we adopt, it can be written as:

$$\rho_i = \sum_{j=1}^N m_j W_{ij} \quad (15)$$

which identifies the natural space interpolation of particle densities according to equation (7).

The pressure term also includes the dissipation contribution. In its original SPH formulation, standing the ideal EoS in the form:

$$p = (\gamma - 1)\rho\epsilon \quad \text{perfect gas equation, (16)}$$

dissipation is given by an artificial viscosity term given by Monaghan (1985, 1992) and Monaghan & Lattanzio (1985), with an appropriate thermal diffusion term which reduces shock fluctuations. It is given by:

$$\eta_{ij} = \alpha_{SPH} \mu_{ij} + \beta_{SPH} \mu_{ij}^2, \quad (17)$$

where

$$\mu_{ij} = \begin{cases} \frac{2h\mathbf{v}_{ij} \cdot \mathbf{r}_{ij}}{(c_{si} + c_{sj})(r_{ij}^2 + \xi^2)} & \text{if } \mathbf{v}_{ij} \cdot \mathbf{r}_{ij} < 0 \\ 0 & \text{otherwise} \end{cases} \quad (18)$$

being c_{si} the sound speed of the i th particle, $\xi^2 \ll h^2$, $\alpha_{SPH} \approx 1$ and $\beta_{SPH} \approx 2$. These α_{SPH} and β_{SPH} parameters of the order of the unity are usually adopted to damp oscillations past high Mach number shock fronts developed by non-linear instabilities (Boris & Book 1973). These α_{SPH} and β_{SPH} values were also adopted by Lattanzio et al. (1985). Smaller α_{SPH} and β_{SPH} values, as adopted by Meglicki et al. (1993), would develop more turbulence in the disc and possibly only one shock front at the impact zone between the infalling particle stream and the returning particle stream at the disc's outer edge. In the physically inviscid SPH gas dynamics, angular momentum transport is mainly due to the artificial viscosity included in the pressure terms as:

$$\frac{p_i^*}{\rho_i^2} + \frac{p_j^*}{\rho_j^2} = \left(\frac{p_i}{\rho_i^2} + \frac{p_j}{\rho_j^2} \right) (1 + \eta_{ij}) \quad (19)$$

where p is the intrinsic gas pressure.

However, looking at a physical origin of the dissipation term, included in the EoS (Lanzafame 2010a,c; Lanzafame et al. 2011), gas pressure can be expressed as:

$$p^* = \frac{\rho}{\gamma} c_s^2 \left(1 - C \frac{n^{-1/3} \nabla \cdot \mathbf{v}}{3c_s} \right)^2, \quad (20)$$

where

$$C = \frac{1}{\pi} \text{arccot} \left(R \frac{v_R}{c_s} \right), \quad (21)$$

where $R \gg 1$. R is a large number describing how much the flow description corresponds to that of an ideal gas: $R \approx \lambda/d$, being $\lambda \propto \rho^{-1/3}$ the molecular mean free path, and being d the mean linear dimension of gas molecules.

3 CONCEPTS ON EXPLICIT AND IMPLICIT INTEGRATION SCHEMES: APPLICATION TO SPH

3.1 Formulations on explicit and implicit generalized three-level integration schemes

Given a physical property A , the mathematical conversion of its time and space derivatives $\partial A / \partial t$, $\partial A / \partial r$, $\partial^2 A / \partial r^2$ is: $(A_k^{n+1} - A_k^n) / \Delta t$, $0.5(A_{k+1}^n - A_{k-1}^n) / \Delta r$ and $0.5(A_{k+1}^n - 2A_k^n + A_{k-1}^n) / \Delta r$, respectively for explicit techniques, while it is $(A_k^{n+1} - A_k^n) / \Delta t$, $0.5(A_{k+1}^{n+1} - A_{k-1}^{n+1}) / \Delta r$ and $0.5(A_{k+1}^{n+1} - 2A_k^{n+1} + A_{k-1}^{n+1}) / \Delta r$, respectively for implicit techniques (Fletcher 1991; Hirsch 1997; LeVeque 2002). In such expressions, n represents the temporal level, while k represents the spatial grid index, according to the versus of

the reference frame. $\Delta t = t^{n+1} - t^n$ and $\Delta r = r_{k+1} - r_k = r_k - r_{k-1} = 0.5(r_{k+1} - r_{k-1})$. Of course other higher order schemes exist, where more time and space levels are considered (Fletcher 1991; Hirsch 1997; LeVeque 2002).

As a useful generalization (Fletcher 1991), the hypothetical equation:

$$\frac{\partial A}{\partial t} + a \frac{\partial A}{\partial r} + b \frac{\partial^2 A}{\partial r^2} + c = 0 \quad (22)$$

can be converted as:

$$\begin{cases} (1 + \lambda) \frac{A_k^{n+1} - A_k^n}{\Delta t} - \lambda \frac{A_k^n - A_{k-1}^{n-1}}{\Delta t} + \\ a \left[(1 - \kappa) \frac{A_{k+1}^n - A_{k-1}^n}{2\Delta r} + \kappa \frac{A_{k+1}^{n+1} - A_{k-1}^{n+1}}{2\Delta r} \right] + \\ b \left[(1 - \kappa) \frac{A_{k+1}^n - 2A_k^n + A_{k-1}^n}{2\Delta r} + \kappa \frac{A_{k+1}^{n+1} - 2A_k^{n+1} + A_{k-1}^{n+1}}{2\Delta r} \right] + \\ c = 0. \end{cases} \quad (23)$$

Whenever the pair $\lambda = 0$ and $\kappa = 0$, such a general expression gives the typical explicit two points forward centred integration scheme (2FCS) for PDE. Instead, for $\lambda = 0$ and $\kappa = 1$ we get a simple full implicit centred three points integration scheme (3FICS). Furthermore, for $\lambda = 0.5$ and $\kappa = 1$ we have a linearized full implicit three points implicit technique (3LFI), while for $\lambda = 0$ and $\kappa = 0.5$ we obtain the well known Crank-Nicholson implicit scheme (Fletcher 1991; Hirsch 1997; LeVeque 2002).

The truncation error (Fletcher 1991) is a function $\propto \Delta r f(\partial^2 A / \partial r^2, \partial^3 A / \partial r^3)$ for upwind 2FCS, as well as 3FICS schemes, while it is $\propto \Delta r^2 f(\partial^3 A / \partial r^3, \partial^4 A / \partial r^4)$ for the other last two implicit techniques.

3.2 SPH in a Semi-Lagrangian explicit-implicit generalized three-level integration scheme

Hydrodynamics in the nonlinear Free Lagrangian SPH approach is currently performed in predictor-corrector explicit schemes, starting from some initial values at time $t = 0$. In the "Leapfrog" scheme, the equations for space and velocity advancement can be written as:

$$r_k^{n+1} = r_k^n + v_k^{n+1/2} \Delta t \quad (24)$$

$$v_{r,k}^{n+1/2} = v_{r,k}^{n-1/2} + a_{r,k}^n \Delta t \quad (25)$$

that can be manipulated into a form which writes particle velocity at integer steps as

$$r_k^{n+1} = r_k^n + v_{r,k}^n \Delta t + \frac{1}{2} a_{r,k}^n \Delta t^2 \quad (26)$$

$$v_{r,k}^{n+1} = v_{r,k}^n + \frac{1}{2} (a_{r,k}^n + a_{r,k}^{n+1}) \Delta t. \quad (27)$$

In this second expression, since particle acceleration a depends on v , it is required an implicit integration for the second equation. In the case of a "Leapfrog" scheme, an "evaluator" phase in the computational scheme needs to be interposed between the two integration procedures, where time derivatives of the various physical quantities are computed. For this reason, this scheme is a so called PEC method, where a Predictor-Evaluator-Corrector procedure is followed by the updating of all integrated values.

Iterative Runge-Kutta methods are also used, both explicit as well as implicit. In such schemes, the integrated

value of the physical property $A_k^{n+1} = A_k^n + S \Delta t$, where S is an estimated weighted average of slopes from the beginning, through some midpoints, toward the end of the time interval. Despite more general than explicit methods, implicit Runge-Kutta schemes are more complicated and dependent on the specific problem. Those Runge-Kutta methods that are diagonally implicit, show a strong stability allowing a significant increase in the time step limit, compared to the explicit methods of the same order (Visbal & Gaitonde 1999; Ketcheson et al. 2009). Here, we do not discuss in detail this specific complex argument, where often some Jacobian matrices need to be inverted. However, even the simple backward Euler ($\lambda = 0, \kappa = 1$), or the Crank-Nicholson ($\lambda = 0, \kappa = 0.5$) methods belong to this category.

The explicit multistep Adams-Bashforth-Moulton PECE explicit integration scheme can also be adopted in SPH, where either the Adams-Bashforth

$$\begin{cases} A_k^{n+1} = A_k^n + \Delta t \frac{\partial A_k^n}{\partial t} \\ A_k^{n+2} = A_k^{n+1} + \frac{\Delta t}{2} \left(3 \frac{\partial A_k^{n+1}}{\partial t} - \frac{\partial A_k^n}{\partial t} \right) \\ A_k^{n+3} = A_k^{n+2} + \frac{\Delta t}{12} \left(23 \frac{\partial A_k^{n+2}}{\partial t} - 16 \frac{\partial A_k^{n+1}}{\partial t} + 5 \frac{\partial A_k^n}{\partial t} \right) \\ A_k^{n+4} = A_k^{n+3} + \frac{\Delta t}{24} \left(55 \frac{\partial A_k^{n+3}}{\partial t} - 59 \frac{\partial A_k^{n+2}}{\partial t} + 37 \frac{\partial A_k^{n+1}}{\partial t} - 9 \frac{\partial A_k^n}{\partial t} \right) \\ A_k^{n+5} = A_k^{n+4} + \frac{\Delta t}{720} \left(1901 \frac{\partial A_k^{n+4}}{\partial t} - 2774 \frac{\partial A_k^{n+3}}{\partial t} + 2616 \frac{\partial A_k^{n+2}}{\partial t} - 1274 \frac{\partial A_k^{n+1}}{\partial t} + 251 \frac{\partial A_k^n}{\partial t} \right), \end{cases} \quad (28)$$

or the Adams-Moulton

$$\begin{cases} A_k^n = A_k^{n-1} + \Delta t \frac{\partial A_k^{n-1}}{\partial t} \\ A_k^{n+1} = A_k^n + \frac{\Delta t}{2} \left(\frac{\partial A_k^{n+1}}{\partial t} + \frac{\partial A_k^n}{\partial t} \right) \\ A_k^{n+2} = A_k^{n+1} + \frac{\Delta t}{12} \left(5 \frac{\partial A_k^{n+2}}{\partial t} + 8 \frac{\partial A_k^{n+1}}{\partial t} - \frac{\partial A_k^n}{\partial t} \right) \\ A_k^{n+3} = A_k^{n+2} + \frac{\Delta t}{24} \left(9 \frac{\partial A_k^{n+3}}{\partial t} + 19 \frac{\partial A_k^{n+2}}{\partial t} - 5 \frac{\partial A_k^{n+1}}{\partial t} + \frac{\partial A_k^n}{\partial t} \right) \\ A_k^{n+4} = A_k^{n+3} + \frac{\Delta t}{720} \left(251 \frac{\partial A_k^{n+4}}{\partial t} + 646 \frac{\partial A_k^{n+3}}{\partial t} - 264 \frac{\partial A_k^{n+2}}{\partial t} + 106 \frac{\partial A_k^{n+1}}{\partial t} - 19 \frac{\partial A_k^n}{\partial t} \right). \end{cases} \quad (29)$$

To apply one of these last two techniques, up to the wished precision, previous derivatives for the same flow elements have to be conserved. Besides, a further evaluator procedure is considered at the end of the predictor-corrector integration scheme, to be a PECE (not a PEC) technique.

What has been discussed is necessary to understand how it is possible to build up a Semi-Lagrangian explicit-

implicit technique. In fact, in this new SPH approach, the first explicit integration scheme is exactly the same that we have adopted, without strictly taking into account the Courant-Friedrichs-Lewy limit for the time step. The adoption of an explicit-implicit backward and forward procedure has been also used by some others (Miranda et al. 1989; Gravouil & Comberscure 2001; Majid et al. 2006; Ying et al. 2008; Ismail et al. 2009), although some recent pure implicit schemes exist (Sahin & Owens 2003, 2006; Mosqueda & Ahmadizadeh 2010), under some strict conditions. We use indifferently both a Leapfrog and an Adams-Bashforth-Moulton scheme as explicit procedure to calculate integrated values to the time level $n+1$. Then, we can simply use iteratively the expression (23) to repeat implicitly the same integrations adopting $\lambda = 0.5$ and $\kappa = 1$ (even the pair $\lambda = 0$ and $\kappa = 1$ can be used to apply the implicit Crank-Nicolson integrations), without any Jacobian matrix inversion mathematical operation. The total number of iterations is of course arbitrary. However, two or three iterations at most are usually enough to get a convergence. We adopt this scheme in 3D along three arbitrary distinct axes (e.g. axes parallel to the X, Y, Z directions), assuming that the real SPH particle stays at the centre of the spatial-temporal (k, n) grid, whose spatial component k is parallel to each arbitrary chosen axis, time by time (Fig. 1). So doing, we assume that both the Eulerian and the Lagrangian spatial derivatives are expressed in the same way in the finite differences scheme and that the correspondence between the temporal Lagrangian derivative d/dt and its corresponding terms in the first row of eq. (23) still holds as for the Eulerian schemes. This can be done because such finite SPH discretizations refer to the moving Lagrangian particle, not to a spatial grid cell. In the conversion of the physical Euler or Navier-Stokes system of equations in its discretized form using eq. (23), it is essential that $dA/dt \propto dF(A)/dr$, where $F(A)$ is the flux density of A . If $dA/dt \propto Adv/dr$ for example, some algebraic operations are needed to put A inside the spatial derivative, within the macros regarding only the implicit integration scheme.

According to this strategy, adopting $(\lambda = 0.5, \kappa = 1)$ the continuity equation, written as:

$$\frac{d\rho}{dt} - \mathbf{v} \cdot \nabla \rho + \nabla \cdot (\rho \mathbf{v}) = 0 \quad (30)$$

in finite difference terms is converted as:

$$\frac{3}{2} \frac{\rho_k^{n+1} - \rho_k^n}{\Delta t} - \frac{1}{2} \frac{\rho_k^n - \rho_k^{n-1}}{\Delta t} - \frac{v_{r,k}^{n+1}}{2\Delta r} (\rho_{k+1}^{n+1} - \rho_{k-1}^{n+1}) + \frac{1}{2\Delta r} (\rho_{k+1}^{n+1} v_{r,k+1}^{n+1} - \rho_{k-1}^{n+1} v_{r,k-1}^{n+1}) = 0, \quad (31)$$

where r is the Cartesian component of the velocity vector. Taking into account that k is a 1D grid number along each X, Y, Z arbitrary directions time by time, we have 3×3 equations to be solved to get as many ρ_k^{n+1} values to be averaged.

In some particular cases, it is better to rewrite the same continuity equation as:

$$\frac{d \ln \rho}{dt} + \nabla \cdot \mathbf{v} = 0. \quad (32)$$

In this case, its finite differences conversion is:

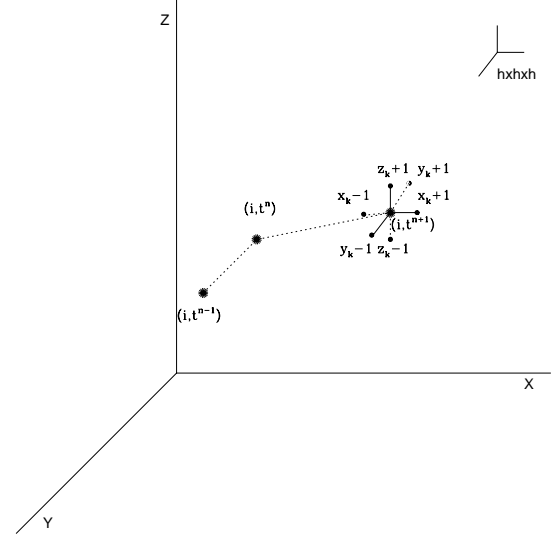


Figure 1. Schematic plot showing the position of the i th SPH particle at time t^{n-1}, t^n and t^{n+1} . At time t^{n+1} the X, Y, Z spatial grid is shown, where physical properties are interpolated, used to perform the implicit 3FICS scheme, together with the information relative to the same particle at previous times.

$$\frac{3}{2} \frac{\ln \rho_k^{n+1} - \ln \rho_k^n}{\Delta t} - \frac{1}{2} \frac{\ln \rho_k^n - \ln \rho_k^{n-1}}{\Delta t} + \frac{1}{2\Delta r} (v_{r,k+1}^{n+1} - v_{r,k-1}^{n+1}) = 0. \quad (33)$$

As far as the energy equation is concerned, written as:

$$\frac{d\rho\epsilon}{dt} + \nabla \cdot [(p + \rho\epsilon) \mathbf{v} - \mathbf{v} \cdot \boldsymbol{\tau}] - \mathbf{v} \cdot \nabla (p + \rho\epsilon) = 0 \quad (34)$$

we have:

$$\frac{3}{2} \frac{\rho_k^{n+1} \epsilon_k^{n+1} - \rho_k^n \epsilon_k^n}{\Delta t} - \frac{1}{2} \frac{\rho_k^n \epsilon_k^n - \rho_k^{n-1} \epsilon_k^{n-1}}{\Delta t} + \frac{1}{2\Delta r} [(p + \rho\epsilon)_{k+1}^{n+1} v_{r,k+1}^{n+1} - (p + \rho\epsilon)_{k-1}^{n+1} v_{r,k-1}^{n+1}] - \frac{1}{2\Delta r} \sum_s (\tau_{r,s,k+1}^{n+1} v_{r,k+1}^{n+1} - \tau_{r,s,k-1}^{n+1} v_{r,k-1}^{n+1}) - \frac{v_{r,k}^{n+1}}{2\Delta r} [(p + \rho\epsilon)_{k+1}^{n+1} - (p + \rho\epsilon)_{k-1}^{n+1}] = 0, \quad (35)$$

where $s = X, Y, Z$.

As far as the momentum equation is concerned, we postpone the inclusion of all explicit external field contributions (e.g. gravitational, electric, magnetic etc.) after having computed the velocity due to the thermodynamics alone. Such contributions can be easily added to the integration as $\Delta t \nabla \Phi_{grav,k}^{n+1}$. According to the same concepts, the momentum equation, without any external field contribution

$$\frac{dv_r}{dt} + \frac{1}{\rho} \left[\frac{dp}{dr} - ((\nabla \cdot \boldsymbol{\tau}) \cdot \mathbf{r}) \right] = 0 \quad (36)$$

is converted as:

$$\frac{3}{2} \frac{v_{r,k}^{n+1} - v_{r,k}^n}{\Delta t} - \frac{1}{2} \frac{v_{r,k}^n - v_{r,k}^{n-1}}{\Delta t} + \frac{p_{k+1}^{n+1} - p_{k-1}^{n+1}}{2\rho_k^{n+1}\Delta r} - \frac{1}{2\rho_k^{n+1}\Delta r} \sum_s (\tau_{s,r,k+1}^{n+1} - \tau_{s,r,k-1}^{n+1}) = 0. \quad (37)$$

Instead, if the same momentum equation is written as:

$$\frac{d\rho\mathbf{v}}{dt} - \mathbf{v} \cdot \nabla(\rho\mathbf{v}) + \nabla \cdot (\rho\mathbf{v}\mathbf{v} - \boldsymbol{\tau}) + \nabla p = 0, \quad (38)$$

its conversion in finite difference terms is:

$$\begin{aligned} & \frac{3}{2} \frac{\rho_k^{n+1} v_{r,k}^{n+1} - \rho_k^n v_{r,k}^n}{\Delta t} - \frac{1}{2} \frac{\rho_k^n v_{r,k}^n - \rho_k^{n-1} v_{r,k}^{n-1}}{\Delta t} - \frac{v_{r,k}^{n+1}}{2\Delta r} (\rho_{k+1}^{n+1} v_{r,k+1}^{n+1} - \rho_{k-1}^{n+1} v_{r,k-1}^{n+1}) + \frac{p_{k+1}^{n+1} - p_{k-1}^{n+1}}{2\Delta r} \\ & - \frac{1}{2\Delta r} \sum_s (\rho_{k+1}^{n+1} v_{r,k+1}^{n+1} v_{s,k+1}^{n+1} - \rho_{k-1}^{n+1} v_{r,k-1}^{n+1} v_{s,k-1}^{n+1}) - \frac{1}{2\Delta r} \sum_s (\tau_{s,r,k+1}^{n+1} - \tau_{s,r,k-1}^{n+1}) = 0. \end{aligned} \quad (39)$$

At last, as far as the Lagrangian position updating equation $d\mathbf{r}/dt = \mathbf{v}$, it could be solved for each $r = X, Y, Z$ component either explicitly as:

$$r_k^{n+1} = r_k^n + v_{r,k} \Delta t \quad (40)$$

or implicitly as:

$$\frac{3}{2} \frac{r_k^{n+1} - r_k^n}{\Delta t} - \frac{1}{2} \frac{r_k^n - r_k^{n-1}}{\Delta t} - v_{r,k}^{n+1} = 0. \quad (41)$$

Throughout these algebraic expressions, some kinetic and thermodynamic quantities have to be computed at $(k+1), (n+1)$ and at $(k-1), (n+1)$ points in the spacetime grid. Adding the i pedex referring to the i th SPH particle, we get:

$$A_{i,k+1}^{n+1} = A_{i,k}^{n+1} + \Delta r_i^{n+1} \sum_{j=1}^N \frac{A_{j,k}^{n+1}}{n_{j,k}^{n+1}} \nabla_i W_{ij}^{n+1}, \quad (42)$$

and

$$A_{i,k-1}^{n+1} = A_{i,k}^{n+1} - \Delta r_i^{n+1} \sum_{j=1}^N \frac{A_{j,k}^{n+1}}{n_{j,k}^{n+1}} \nabla_i W_{ij}^{n+1}. \quad (43)$$

Thus, the SPH technique is again used to compute the spatial gradients ∇A_i (e.g, gradients of density, pressure and so on) to the i th SPH particle. For the sake of simplicity, even though Δr_i is an arbitrary length, we adopt $\Delta r_i = h_i$, whatever is the time level n .

Once $\rho_{i,s}^{n+1}, \epsilon_{i,s}^{n+1}, v_{r,i,s}^{n+1}$ ($r = X, Y, Z$) are given at time $n+1$ for the i th SPH particle for $s = 1, 2, 3$ in 3D, the final values $\rho_i^{n+1}, \epsilon_i^{n+1}, v_{r,i}^{n+1}$ in 3D are calculated as: $A_i^{n+1} = \sum_s A_{i,s}^{n+1}/3$.

In this notation, notice that the grid index k identifies the i th particle along the 1D computational arbitrary spatial line (here X, Y , or Z) in 3LFI. Indexes $k+1$ and $k-1$ refer to the interpolation spatial points "ahead" and "behind" the same i th SPH particle along such an axis. Instead, the s index, like the r index, refers to the direction of the 1D arbitrary computational spatial line. In our notation, s follows

r , but it could be different, in principle. Therefore, as an example, we compute $\rho_{i,x}^{n+1}, \rho_{i,y}^{n+1}, \rho_{i,z}^{n+1}, \epsilon_{i,x}^{n+1}, \epsilon_{i,y}^{n+1}, \epsilon_{i,z}^{n+1}$ that means the density and the thermal energy per unit mass on the i th particle, at time $n+1$, along the x, y, z lines (along the 1, 2, 3 arbitrary lines). Moreover, $v_{x,i,x}^{n+1}, v_{x,i,y}^{n+1}, v_{x,i,z}^{n+1}, v_{y,i,x}^{n+1}, v_{y,i,y}^{n+1}, v_{y,i,z}^{n+1}, v_{z,i,x}^{n+1}, v_{z,i,y}^{n+1}, v_{z,i,z}^{n+1}$ mean the x, y, z velocity components on the i th particle, at time $n+1$, along the x, y, z lines (along the 1, 2, 3 arbitrary lines).

The strategy adopted in this explicit-implicit Semi-Lagrangian scheme is similar, for some aspects to that adopted to solve ordinary differential equations (ODE), even up to the second order in some explicit and implicit three point methods by some authors (Majid et al. 2006; Ismail et al. 2009).

3.3 Choice of a time step for an SPH Semi-Lagrangian explicit-implicit scheme

The Courant-Friedrichs-Lewy condition on the time step progression to solve PDE and ODE for explicit integration techniques offers a temporal reference where numerical solutions are both stable and convergent with the mathematical solutions. Unfortunately, such a temporal reference is still debated for implicit integration of PDE and ODE (Staniforth & Côté 1991).

For SPH technique, the Courant-Friedrichs-Lewy time limiter is given by:

$$\Delta t_{CFL} = C \min_{i=1,N} \left[\frac{h}{v_{sig,ij}}, (\nabla \cdot |\mathbf{v}|_i)^{-1}, \left(\frac{h}{|\mathbf{a}|_i} \right)^{1/2} \right], \quad (44)$$

being $v_{sig,ij}$ the signal transmission velocity between close particles i and j within the SPH spatial resolution length h (Monaghan 1985, 1992, 1997; Whitehurst 1995) also including the sound velocity c_{si} , $|\mathbf{a}|_i$ the full acceleration for the i th SPH particle. C is a number of the order of 0.2–0.5.

Since in a correct Free Lagrangian particle fluid dynamics particles cannot interpenetrate with each other, an "absolute" time step limit should be the "kinetic" value:

$$\Delta t_k = C \min_{i=1,N} \left[(\nabla \cdot |\mathbf{v}|_i)^{-1}, \left(\frac{h}{|\mathbf{f}|_i} \right)^{1/2} \right], \quad (45)$$

where $|\mathbf{f}|_i$ is the force per unit mass due to gravitational and to pressure terms only. However, such a larger limiter, could be correct for a Semi-Lagrangian implicit SPH hydrodynamics only for weak shock flows. To overcome such a difficulty, we consider the limiter:

$$\Delta t_l = (\Delta t_{CFL} \Delta t_k)^{1/2}, \quad (46)$$

which corresponds to the geometric mean of the previous two. This choice both prevents the numerical collapse of the time step to be used, and gives a good hydrodynamics far from the risk of getting wrong solution for supersonic flows that occur when $\Delta t \sim \Delta t_k$. Of course, for very extreme situations, even this time step limiter cannot be correctly used, because of the lack of the existence of a temporal top limit for implicit integrations techniques. The ratio $\Delta t_k/\Delta t_{CFL}$ is always ≥ 1 . However, whenever $\Delta t_k/\Delta t_{CFL} > 400$ (e.g. $\Delta t_l > 20\Delta t_{CFL}$), some consistent deviations from the correct solutions are recorded. These deviations are much better confined in so far as $\Delta t_k/\Delta t_{CFL} \leq 10$.

The choice of a time step for a Semi-Lagrangian explicit-implicit scheme is totally arbitrary, of course. We could also proceed simply considering an implicit $t^{n+1} - t^n = \Delta t \propto \Delta t_{CFL}$, whose parameter of proportionality should be found. However, in this case, some cases should be excluded. In fact, for example, if we establish that this number is of the order of 10, this number should be not correct for non collisional supersonic flows when $\Delta t_k/\Delta t_{CFL} \simeq 1$. Hence, a $\Delta t_l \propto \Delta t_{CFL}$ should be a general rule in so far as the constant of proportionality should be found case by case. Instead, formulation (46) automatically better correlates the implicit Δt to Δt_{CFL} and to Δt_k . It is true that sometimes we could also work using a larger implicit Δt , but some cautions are needed.

Given these definitions, the time step adopted for the Semi-Lagrangian explicit-implicit scheme discussed in SS3.2 is: $t^{n+1} - t^n = \Delta t = \Delta t_l - \Delta t_{CFL}$, being Δt_{CFL} used in the first explicit step. Whenever $\Delta t = 0$, only the explicit technique is applied.

4 1D BLAST WAVE TESTS

The behaviour of shock fronts moving in the prevailing flow is analytically described by the Rankine-Hugoniot "jump conditions" (LeVeque 1992, 2002; Hirsch 1997; Toro 1999; Batchelor 2000). These conditions are obtained by spatially integrating the 1D hyperbolic Euler equations across the discontinuity between the two flow regimes left-right in their Eulerian formalism:

$$\frac{\partial \rho}{\partial t} = -\frac{\partial}{\partial x}(\rho v) \quad (47)$$

$$\frac{\partial \rho v}{\partial t} = -\frac{\partial}{\partial x}(\rho v^2 + p) \quad (48)$$

$$\frac{\partial \rho E}{\partial t} = -\frac{\partial}{\partial x}E, \quad (49)$$

where $E = \rho v^2/2 + \epsilon + p/\rho$, whose conservative analytical form can be synthesized as:

$$\frac{\partial w}{\partial t} = -\frac{\partial}{\partial x}f(w). \quad (50)$$

In the limit of zero thickness of the shock discontinuity,

$$s(w_l - w_r) = f(w_l) - f(w_r). \quad (51)$$

Under these conditions a requirement for a unique single-valued solution is that the solution should satisfy the Lax entropy condition (LeVeque 1992, 2002; Hirsch 1997; Toro 1999) $f'(w_l) < s < f'(w_r)$, where $f'(w_l)$ and $f'(w_r)$ are the characteristic speeds at upstream and downstream conditions, respectively. The integrated form of the Rankine-Hugoniot jump conditions are:

$$s(\rho_l - \rho_r) = \rho_l v_l - \rho_r v_r \quad (52)$$

$$s(\rho_l v_l - \rho_r v_r) = (\rho_l v_l^2) - (\rho_r v_r^2) \quad (53)$$

$$s(\rho_l E_l - \rho_r E_r) = \rho_l v_l E_l - \rho_r v_r E_r, \quad (54)$$

It is shown, after some algebraic passages, that the shock speed is:

$$s = v_l + c_{sl} \left[1 + \frac{\gamma + 1}{2\gamma} \left(\frac{p_r}{p_l} - 1 \right) \right]^{1/2} \quad (55)$$

where $c_{sl} = (\gamma p_l / \rho_l)^{1/2}$. In the case of stationary shocks, being both the upstream and downstream pressures positive, there is an upper limit on the density ratio: $\rho_l / \rho_r \leq (\gamma + 1) / (\gamma - 1)$. However, this limit is currently applied also to non steady shocks.

Whenever in a shocktube the ratios $p_1/p_1 = \epsilon_1/\epsilon_2 \gg 1$, and consequently $\rho_1/\rho_2 = 1$, and $v_1 = v_2 = 0$, such a discontinuity is called a "blast wave". Fig. 2 shows a comparison of both explicit and implicit SPH results together with the so called analytical solution. Such an analytical solution is considered corrected in so far as $\rho_1/\rho_2 \leq (\gamma + 1) / (\gamma - 1)$. In the SPH blast wave test here considered, $p_1/p_1 = \epsilon_1/\epsilon_2 = 10^4$, while the SPH particle resolution length is $h = 5 \cdot 10^{-2}$. The whole computational domain is built up with 2001 particles from $X = 0$ to $X = 100$, whose mass is different, according to the shock initial position. At time $T = 0$ all particles are motionless and the adiabatic index $\gamma = 5/3$, while the ratios $\rho_1/\rho_2 = 1$. The first 5 and the last 5 particles of the 1D computational domain, keep fixed positions and do not move. The choice of the final computational time is totally arbitrary, since the shock progresses in time. Initial values of v , ρ and ϵ at time $T = 0$ are shown at the left-right edges of each plot of the same Fig. 2.

Fig. 2 shows that both SPH results globally compare with each other and that they also compare with the analytical solution wherever $\rho_1/\rho_2 \leq (\gamma + 1) / (\gamma - 1)$, that is wherever the Rankine-Hugoniot jump conditions hold. Beyond this limit, even the so called analytical solution is considered incorrect. Being $\gamma = 5/3$, the comparison is meaningful within $\rho_1/\rho_2 \leq 4$. Both SPH (explicit and implicit) results are in a good comparison with the analytical solution. Discrepancies involve only 4 particles at most, with the exception of numerical solutions corresponding to analytical vertical profiles regarding thermal energy where, for both SPH solutions, discrepancies are larger. As Fig. 2 clearly shows, both the SPH numerical solutions suffer from some small well known instabilities, especially in the proximity of discontinuities (Gibbs 1898, 1899; Monaghan 1997) as far as the velocity profile is concerned. Such effect comes out whenever a spatial high resolution is working together with an explicit handling of dissipation through an artificial viscosity damping to solve the Riemann problem of flow discontinuities. A low spatial resolution hides this effect because of the higher artificial damping due to a higher particle resolution length h (eqs. 17-18). The higher the spatial resolution (the smaller h), the higher the "blimp" instabilities. Moreover, in SPH, even the choice of the arbitrary parameters α and β should be linked to the specific physical problem. Another way for reduction of instabilities is possible (Lanzafame 2010a,c; Lanzafame et al. 2011) if the damping is strictly locally physical, using eqs. (20, 21) instead of eq. (16) for the perfect gases EoS. An effective reduction of "blimp" effects is obtained, especially for 1D blast waves, where strong discontinuities in the flow deeply affect the SPH numerical solution producing intrinsic numerical instabilities close to the propagating discontinuities.

Apart from the accordance between analytical and numerical (explicit and implicit) results, what is remarkable is the fact that implicit results are obtained in about half of cpu time in implicit SPH approach, compared to the traditional explicit SPH, adopting the time step criterion expressed by eq. (46). The final time configuration at time

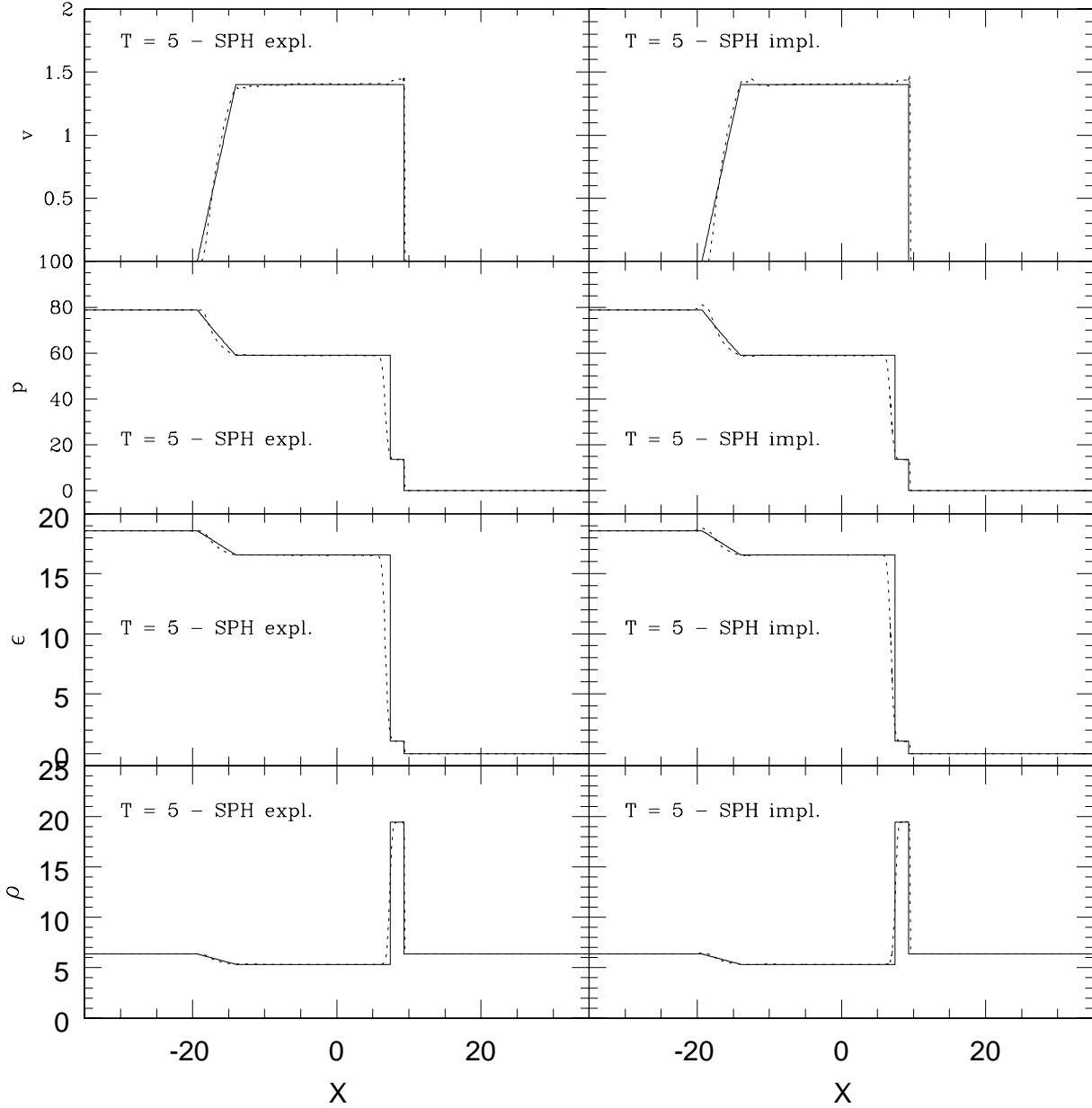


Figure 2. 1D blast wave test regarding the comparison of both explicit (left size) and implicit (right size) SPH results to analytical (solid line) results. Density ρ , thermal energy ϵ , pressure p and velocity v are plotted at time $T = 5$. Density and thermal energy of particles initially at rest at time $T = 0$ refer to values plotted at the two edges for each plot. The initial velocity is zero throughout.

$T = 5$ is an evolved configuration well beyond the initial instants from $T = 0$. At the final time configuration at time $T = 5$ the ratio $\Delta t_l / \Delta t_{CFL} \sim 1.6$. Since the beginning of a blast wave simulation, this ratio ~ 2 is globally held as an order of magnitude. This implies that in the particular case of a detonation, the criterion adopted on the time step progress (Δt_l in §3.3) shows accordance with analytical results without any difficulties, being $\Delta t_l / \Delta t_{CFL}$, well within the factor of 6 discussed in §1. Notice that these accords are not verified at the 1st time step, where an explicit integration scheme must be applied.

5 SIMULATIONS OF A 3D ACCRETION DISC AROUND A MBH IN A CLOSE BINARY

We compare results of both inviscid and viscous stationary disc structures performing SPH simulations whose integration schemes are both explicit and implicit in low compressibility ($\gamma = 1.3$) with the aim of getting a physically well-bound accretion disc around a MBH a close binary. Previous preliminary results on this theme were published (Lanzafame & Belvedere 2001, 2002, 2005) both in 2D and in 3D.

The characteristics of the binary system are determined by the masses of the MBH and of its companion star and their separation. We chose to model a system in which the mass M_1 of the primary MBH and the mass M_2 of the secondary subgiant star are equal to $32M_\odot$ and $1M_\odot$, respectively and their mutual separation is $d_{12} = 10^8 \text{ Km}$. The primary's potential well is totally empty at the beginning of each simulation at time $T = 0$. The injection gas velocity at L1 is fixed to $v_{inj} \simeq 130 \text{ Km s}^{-1}$ while the injection gas temperature at L1 is fixed to $T_o = 10^4 \text{ K}$, taking into account, as a first approximation, the radiative heating of the secondary surface due to radiation coming from the disc. Gas compressibility is fixed by the adiabatic index $\gamma = 1.3$. Supersonic kinematic conditions at L1 are discussed in Lanzafame (2008, 2009); Lanzafame et al. (2006), especially when active phases of CB's are considered. However, results of this paper are to be considered as a useful test to check whether disc structures (viscous and non) show the expected behaviour. The reference frame is centred on the primary compact star, whose rotational period, normalized to 2π , coincides with the orbital period of the binary system. This explains why in the momentum equation (eq. 2), we also include the Coriolis and the centrifugal accelerations.

Pressure, density, temperature and velocity are six unknowns to be found. Therefore we solve the continuity, momentum, energy, and EoS equations. In order to make our equations dimensionless, we adopt the following normalization factors: $M = M_1 + M_2$ for masses, $d_{12} = 10^{11} \text{ cm}$ for lengths, $v_o = (G(M_1 + M_2)/d_{12})^{1/2}$ for speeds, so that the orbital period is normalized to 2π , $\rho_o = 10^{-9} \text{ g cm}^{-3}$ for the density, $p_o = \rho_o v_o^2 \text{ dyn cm}^{-2}$ for pressure, v_o^2 for thermal energy per unit mass and $T_o = (\gamma - 1)v_o^2 m_p K_B^{-1}$ for temperature, where m_p is the proton mass and K_B is the Boltzman constant. The adopted Kernel resolving power is $h = 5 \cdot 10^{-3}$ throughout. The geometric domain, including disc particles, is a sphere of radius 1, centred on the primary MBH. The rotating reference frame is centred on the compact primary and its rotational period equals the orbital one. We simulated the physical conditions at the inner and at the outer edges as follows:

a) inner edge:

the free inflow condition is realized by eliminating particles flowing inside the sphere of radius 10^{-2} , centred on the MBH. Although disc structure and dynamics are altered near the inner edge, these alterations are relatively small because they are counterbalanced by a high particle concentration close to the inner edge in supersonic injection models.

b) outer edge:

the injection of "new" particles from L1 towards the interior of the primary Roche Lobe is simulated by generating them in fixed points, called "injectors", symmetrically placed within an angle having L1 as a vertex and an aperture of $\sim 57^\circ$. Normally, as adopted since our first paper on SPH accretion disc in CB (Molteni et al. 1991), the radial elongation of the whole ensemble of injectors is $\sim 10h$. The initial injection particle velocity is radial with respect to L1. In order to simulate a constant and smooth gas injection, a "new" particle is generated in the injectors whenever "old" particles leave an injector free, inside a small sphere with radius h , centred on the injector itself. Particle masses are determined by the assumed local density at

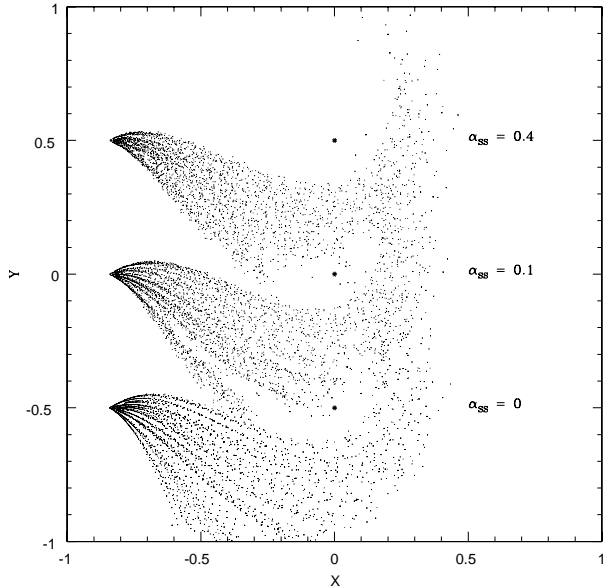


Figure 3. XY plots of the injected particle stream for the non viscous ($\alpha_{SS} = 0$) and the two disc models ($\alpha_{SS} = 0.1$ and $\alpha_{SS} = 0.4$) at time $t = 1$. The central MBH position is also shown. Notice that the Y positions are shifted for $\alpha_{SS} = 0$ and for $\alpha_{SS} = 0.4$.

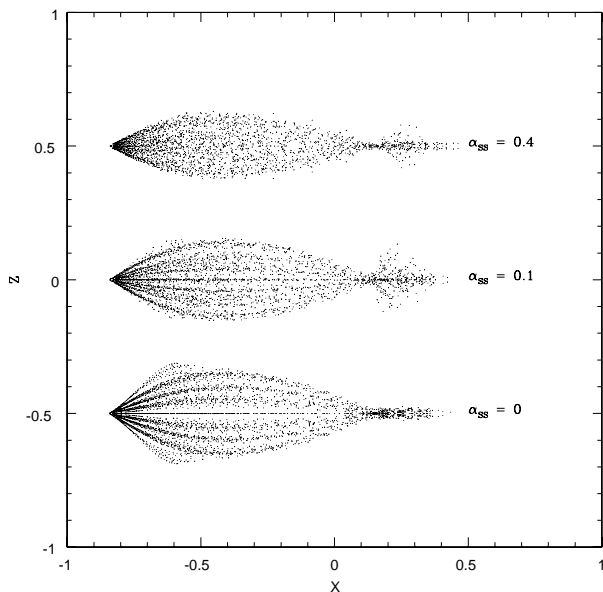


Figure 4. XZ plots of the injected particle stream as in Fig.3.

the inner Lagrangian point L1: $\rho_{L1} = 10^{-9} \text{ g cm}^{-3}$ (as typical stellar atmospheric value for the secondary star), equal to $m = \rho_{L1}(hd_{12})^3/(M_1 + M_2)$.

The adoption of supersonic mass transfer conditions from L1 is fully discussed in Lanzafame (2008, 2009), where disc instabilities, responsible for disc active phases of CB are discussed in the light of local thermodynamics. Whenever a relevant discrepancy exists in the mass density across the inner Lagrangian point L1 between the two stellar Roche

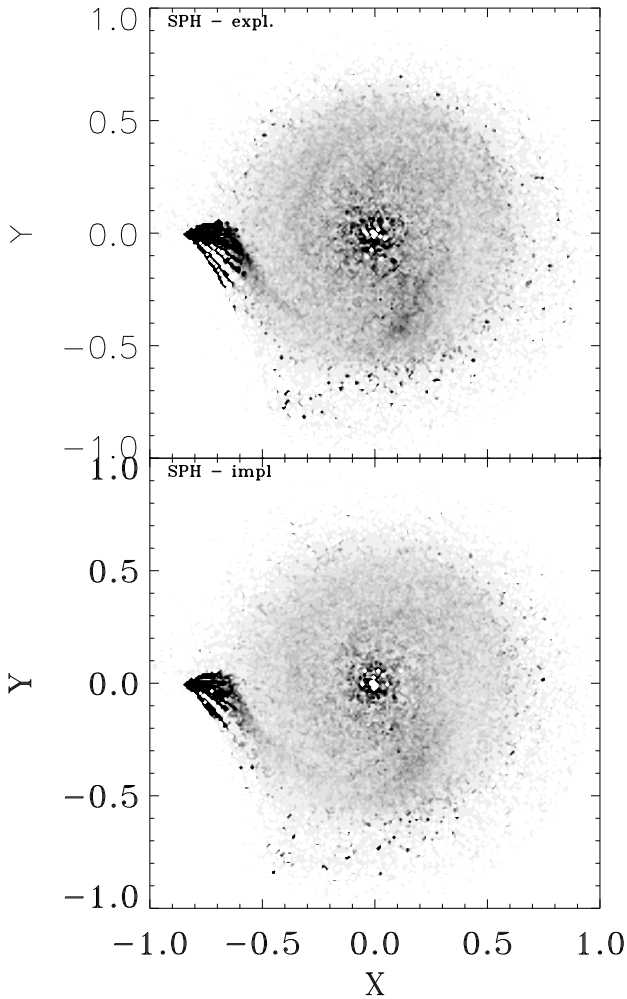


Figure 5. XY plots of 64 greytones density ρ isocontours of the non viscous 3D SPH disc modelling in a microquasar. Explicit SPH results compare with SPH implicit ones.

lobes, a supersonic mass transfer occurs as a consequence of the momentum flux conservation. The same result can also be obtained (Lubow & Shu 1975) by considering either the restricted problem of three bodies in terms of the Jacobi constant or the Bernoulli's theorem. Moreover, and this is the most important thing, we need to compare 3D disc models where Δt_{CFL} and Δt_k could be significantly different. This condition is searched for since the injection conditions at L1, favouring violent collisions among low compressibility ($\gamma = 1.3$) particles moving around a MBH, rising up particle heating at expense of the kinetic + gravitational energies. These conditions make much smaller the thermal contribution in Δt_{CFL} evaluation compared to the kinetic contribution throughout the disc, especially when viscous heating or other forms of heating are considered. Thus when $\Delta t_i / \Delta t_{CFL} \gg 1$, a significant deviation in the implicit solutions would affect the whole result, up to compromising the numerical stability. A sensible reduction in Δt_{CFL} even happens whenever other forms of signal transmission velocity (e.g. the Alfvén speed) are also taken into account.

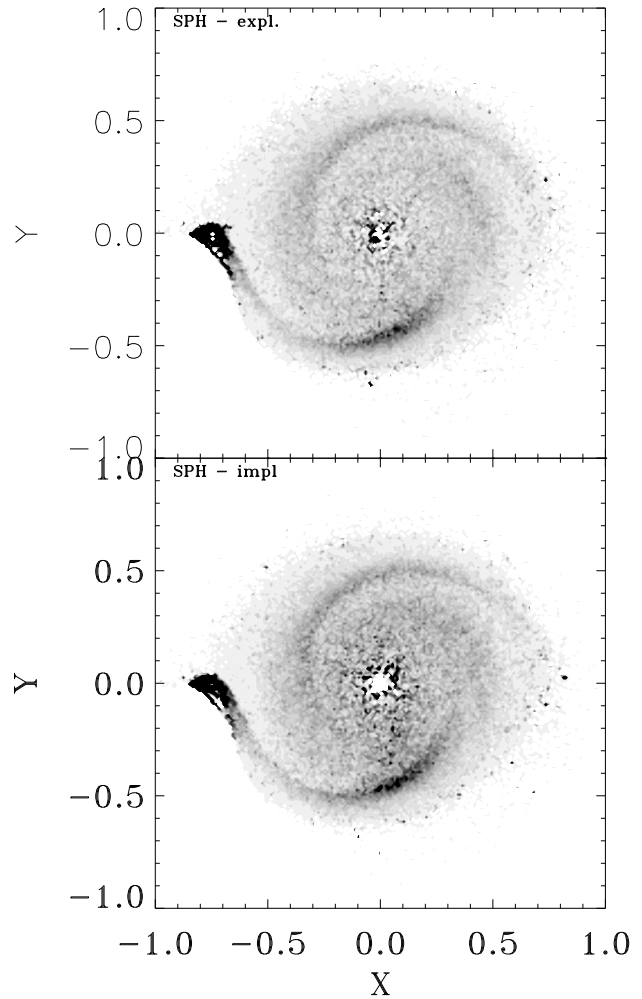


Figure 6. XY plots of 64 greytones density ρ isocontours of the $\alpha_{SS} = 0.1$ viscous 3D disc modelling in a microquasar. Explicit SPH results compare with SPH implicit ones.

The first viscosity coefficient (eq. 10) in the viscous disc models is related to the Shakura and Sunyaev parametrization (Shakura 1972; Shakura & Sunyaev 1973) as: $\eta_v = \rho \alpha_{SS} c_s H$, being H the local disc thickness. The second viscosity coefficient, related to the bulk viscosity is not taken into account for the sake of simplicity. Two viscous disc models are considered, whose $\alpha_{SS} = 0.1$ and whose $\alpha_{SS} = 0.4$. These values are in accordance with the typical and with the maximum α_{SS} compatible with both astrophysical observations (King et al. 2007) and with laboratory experiments (Abolmasov & Shakura 2009). These disc models are also compared with the non viscous disc model counterpart, taken as a reference model.

Fig. 3 and 4 show three XY and XZ plots of the injected stream from L1 at time $t = 1$ for the three disc models. The greater compactness of the injected flow of particles is visible with the increase of the viscosity parameter as a result of the sticking viscous effect. The large stream geometric spread is mainly due to the low compressibility here adopted ($\gamma = 1.3$), while the wide initial circulariza-

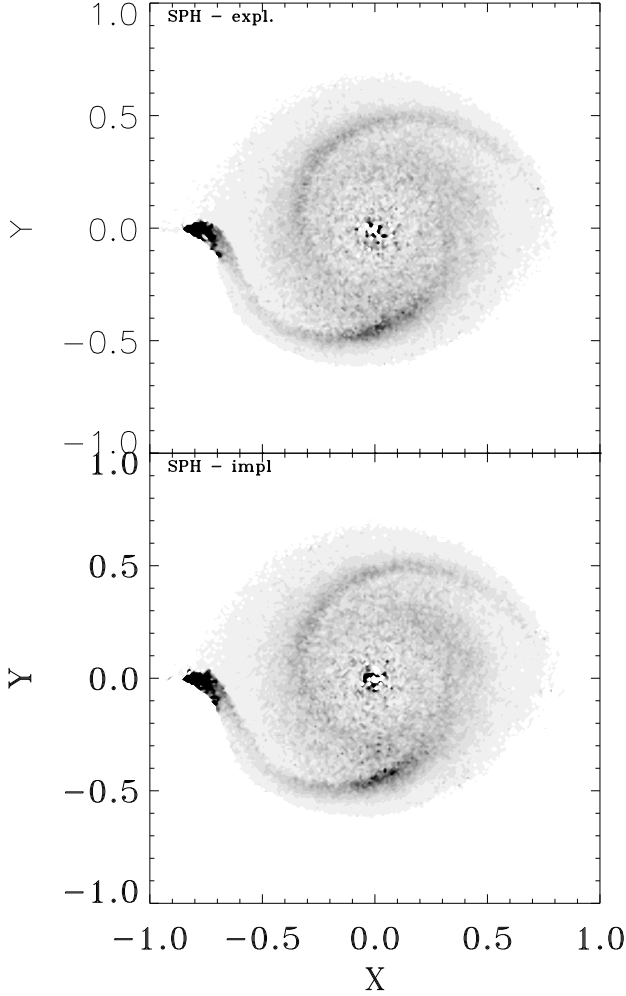


Figure 7. XY plots of 64 greytones density ρ isocontours of the $\alpha_{SS} = 0.4$ viscous 3D disc modelling in a microquasar. Explicit SPH results compare with SPH implicit ones.

tion radius is explained by the high angular momentum at L1 of the injected flow. These initial kinematic conditions affect the whole disc structure and kinematics throughout the simulations. In fact, the injected gas stream yields an impassable boundary of the outer disc edge itself and a significant fraction of the disc's ejection flow comes from this side of the outer disc edge. Besides, a wide spray of direct cold injected flow above and below the mean disc plane also plays a role.

Figs. 5, 6 and 7 show a comparison of explicit and implicit SPH disc structures for the non viscous and the viscous models whose $\alpha_{SS} = 0.1$ and 0.4 , respectively. All explicit and implicit structures impressively compare with each other, as well as their injection, ejection and accretion rates, whose values are in the order of $\sim 10^{21} g s^{-1}$, $6.5 \cdot 10^{20} g s^{-1}$ and $3.5 \cdot 10^{20} g s^{-1}$, respectively for the inviscid disc models, of $\sim 7.8 \cdot 10^{20} g s^{-1}$, $3.6 \cdot 10^{20} g s^{-1}$ and $4.2 \cdot 10^{20} g s^{-1}$, respectively for the $\alpha_{SS} = 0.1$ viscid disc models, of $\sim 5.9 \cdot 10^{20} g s^{-1}$, $2.6 \cdot 10^{20} g s^{-1}$ and $3.3 \cdot 10^{20} g s^{-1}$, respectively for the $\alpha_{SS} = 0.4$ viscid disc

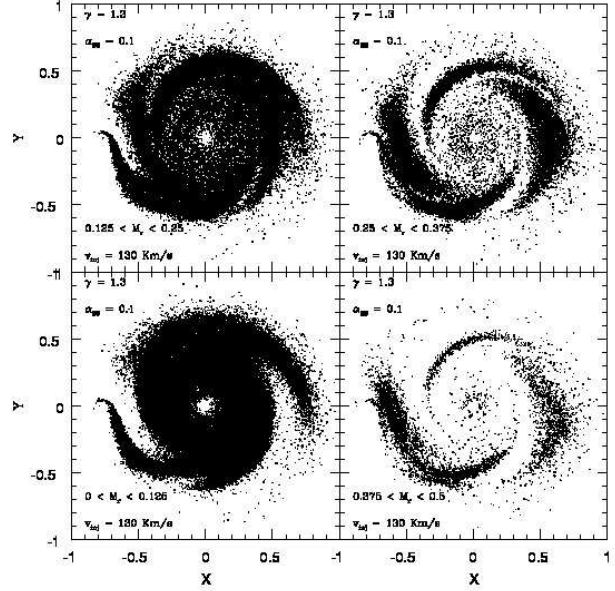


Figure 8. XY plots of the subsonic spiral kinematics of the $\alpha_{SS} = 0.1$ viscous 3D disc in a microquasar. Selection in the radial Mach number M_r are shown in each panel.

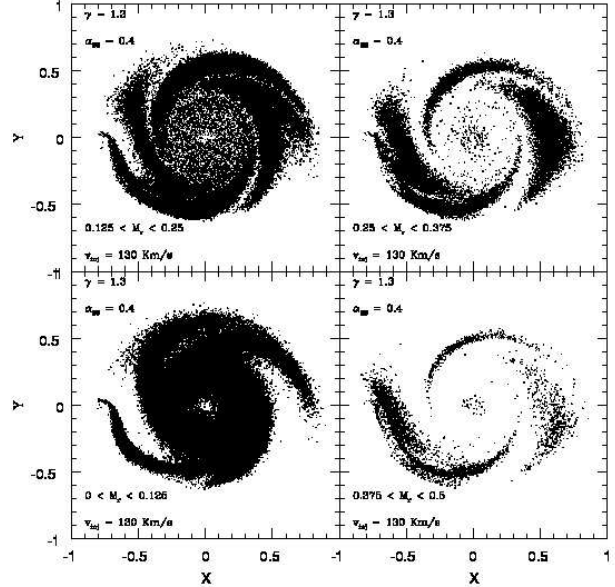


Figure 9. XY plots of the subsonic spiral kinematics of the $\alpha_{SS} = 0.4$ viscous 3D disc in a microquasar. Selection in the radial Mach number M_r are shown in each panel.

models. The total number of disc particles are of the order of 135000, 143000 and 125000 particles, respectively in steady state conditions when the mass of the disc is statistically unchanged.

Even though disc models refer to a low compressibility regime ($\gamma = 1.3$), the primary's MBH Roche lobe is large and deep enough to favour a disc consistency even in the non viscous disc model. This is a first result, different from those relative to low mass binaries, where SPH mod-

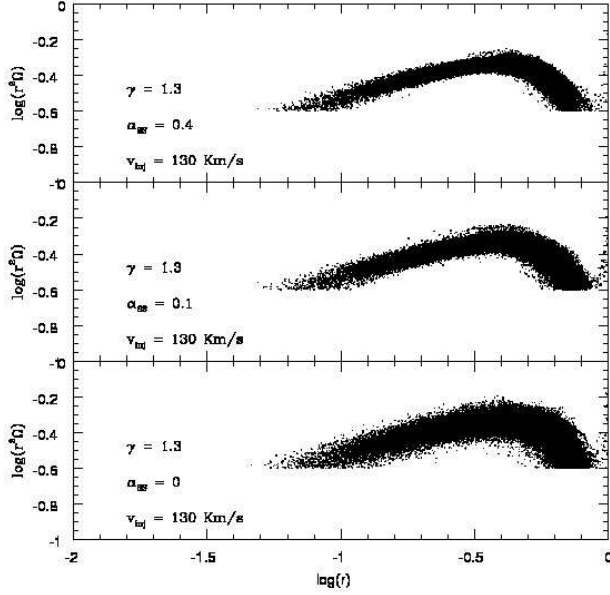


Figure 10. Radial distribution of the specific angular momentum in a logarithmic scale.

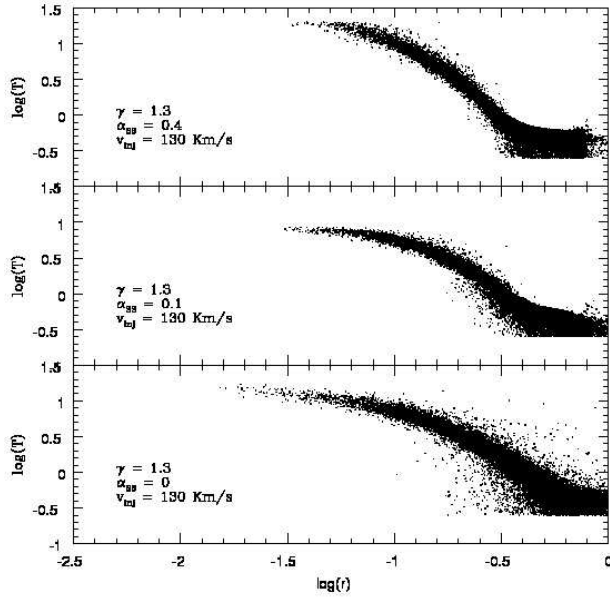


Figure 11. Radial distribution of temperature in a logarithmic scale.

els yield scarcely populated low compressibility non viscous structures (Molteni et al. 1991; Lanzafame et al. 1992). Although finalized to a different strategy, a statistically significant 2D structure of the disc around a MBH were obtained by (Lanzafame & Belvedere 2005).

The collisional push exerted by the flow coming from L1 on the outer edge of the disc yields an effective perturbation generating a global disc's elliptic geometry in the viscous cases. As a consequence, spiral density patterns characterize SPH viscous disc models around MBH, as well depicted in Fig. 6 and 7. Instead, possible spiral patterns are not

well resolved, or they do not well develop in the SPH non viscous model because of the inadequacy of dissipation able to numerically resolve shock fronts in the low compressibility flow and because the stream flow from L1 is too sparse in order to exert an effective localized push at the disc's outer edge. In these two last figures in particular, relative to the two physically viscous models, two main spiral patterns in the density are evident, even if the glimmer of the appearance of a third one is also shown. These facts are recorded in 3D modelling. On the contrary, spiral structures around MBH, as well as spiral shocks in the disc's radial flow, are normally seen in the 2D non viscous low compressibility modelling (Lanzafame & Belvedere 2005). In the case of low mass close binaries, SPH low compressibility viscous disc models are not able to show any spiral pattern because of several shortcomings in the method, especially when free edge conditions are considered (Lanzafame 2010b).

The better compactness of the entire elliptical viscous disc structure, not only yields disc's spiral density profiles, but contextually also a spiral radial flow kinematics. In these low compressibility viscous models, this is a subsonic kinematics, as shown in Figg. 8 and 9 where a selection in the radial Mach number is made. The tendency should be to produce spiral shocks which should appear either increasing the flow compressibility modelling (decreasing γ) (Chakrabarty 1992), or altering the stellar mass ratio or the initial injection kinematics in order to simulate a mass transfer flow from L1 where the radial kinematics is more enhanced than the tangential one. The higher are the kinetic energy and the initial angular momentum, the better is the coming out of spiral structures and shocks (Lanzafame et al. 2000, 2001). This is a consolidated result that has emerged for low mass binary systems. However, in the case of a microquasar, where the primary component is a MBH, a large initial angular momentum and large Coriolis and centrifugal terms favour too much an initial tangential kinematics at the cost of the radial one.

A further comprehension of disc structure and kinematics is shown in Fig. 10 and 11, where the radial distribution of the specific angular momentum and the radial distribution of temperature are respectively shown in a logarithmic scale. Two details come out from these pictures. The first one is that the inner disc regions are less populated of particles in the two viscous models. This effect, due to the enhanced radial viscous transport, makes the radial profile of these two distributions more "flat" compared to that relative to the non viscous distributions. The second particular that appear from these two pictures is that the slopes of the two radial distributions are lesser than $r^2\Omega \propto r^{1/2}$ and $T \propto r^{-3/4}$ relative to the "standard disc model". The temperature radial profile is even flat for a large portion of the external part of the discs. This result is a consequence of the wide geometric opening of the injected flow coming from L1 (Figg. 3-4), where colder and higher radial flow in the disc bulk mix with hotter flows transported from the disc outer edge toward the central accretor. As a consequence, looking from the outer disc edge toward the centre of the disc, both the temperature radial increase and the specific angular momentum decrease are lower than $T \propto r^{-3/4}$ and $r^2\Omega \propto r^{1/2}$ laws, even though the viscous heating effect in the disc bulk and in its inner regions is remarkable especially for the $\alpha_{SS} = 0.4$.

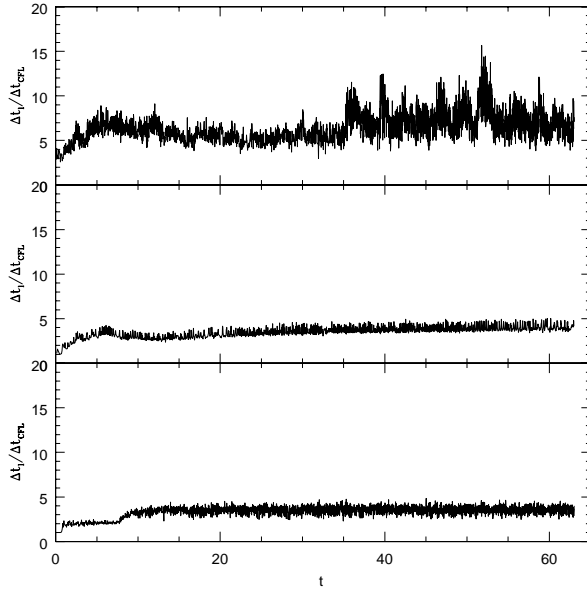


Figure 12. $\Delta t_i/\Delta t_{CFL}$ as a function of time t for the three simulated 3D accretion discs. The panel at the bottom refers to the $\alpha_{SS} = 0$ non viscous model. $\alpha_{SS} = 0.1$ (middle panel) as well as $\alpha_{SS} = 0.4$ (top panel) results are also reported.

6 CONCLUDING REMARKS

From the numerical point of view, a successful Semi-Lagrangian explicit-implicit integration numerical scheme is here applied for the SPH method. This scheme can also be applied to Free Lagrangian schemes in principle. Comparison to results obtained working with explicit numerical schemes shows an impressive convergence of results. Traditionally, numerical schemes in such explicit-implicit approaches are stable and show a convergence when the adopted implicit time step is larger than the explicit one by up to 6 times (Staniforth & Côté 1991). In this study, correlating our implicit time stepping to the Courant-Friedrichs-Lewy explicit time stepping Δt_{CFL} and to the kinematic time stepping Δt_i , we report consistent and stable results both for a test case regarding a 1D blast wave model and for 3D low compressibility accretion disc models around a MBH in a microquasar. This choice, in particular for the viscous modelling is motivated to stress the validity of the implicit technique we described. Convergence and consistency of results is recorded up to a ratio of 15 as shown in Fig. 12 for the $\alpha_{SS} = 0.4$ physically viscous accretion disc modelling, where $\Delta t_i/\Delta t_{CFL}$ is reported as a function of time for the implicit results for the three simulated discs. This has the evident advantage that working in such an explicit-implicit scheme we can obtain meaningful results in a much shorter time than working adopting the Courant-Friedrichs-Lewy time stepping. In particular we yield implicit results for the $\alpha_{SS} = 0.1$ and $\alpha_{SS} = 0.4$ discs in two weeks of cpu time using a serial code on a system based on an AMD Opteron cpu instead of times of the order of 5 months on the same hardware working in explicit integration technique.

From the astrophysical point of view, a well-bound accretion disc appears in a microquasar even if a non viscous

- low compressibility modelling. This is allowed because of the strong gravitational field of the central MBH prevailing on the repulsive pressure forces. In these low compressibility models the kinematic of the radial flow stays subsonic throughout even if the physical viscous contribution is also taken into account. For the physically viscous models, two main spiral patterns in the density flow clearly appear mainly as a consequence of the elliptical morphology of the entire disc structure and the disc's outer edge is better shaped. A possible third spiral profile can also appear. The disc structures all deviate from that of the disc standard model because of the vertical inflow of cold gas coming from L1.

ACKNOWLEDGMENTS

We thank Dr. P. Leto of the INAF - Osservatorio Astrofisico di Catania for some helpful interventions that improved the presentation of the paper.

REFERENCES

- Abolmasov, P., Shakura, N.I., 2009, AN, 7, 737
- Ardeljan, N.V., Bisnovatyi-Kogan, G.S., Kosmachevskii, K.V., Moiseenko, S.G., 1996, A&ASS, 115, 573
- Batchelor, K., 2000, "An introduction to fluid dynamics", Cambridge Univ. Press
- Boris, J.P., Book, D.L., 1973, JCoPh, 11, 38
- Chakrabarty, S.K., 1992, MNRAS, 259, 410
- Courant, R., Friedrichs, K., Lewy, H., 1928, Mathematische Annalen, 10, 32
- Courant, R., Friedrichs, K., Lewy, H., 1967, (Engl. transl.) IBM Journal & AEC Report NYO-7689, 215
- Flebbe, O., Münzel, H., Riffert, H., Herold, H., 1994a, Mem. S.A.It, 65, 1049
- Flebbe, O., Münzel, H., Herold, H., Riffert, H., Ruder, H., 1994b, ApJ, 431, 754
- Fletcher, C.A.J., 1991, "Computational techniques for fluid dynamics", Springer
- Gibbs, J.W., 1898, Nature, 59, 200
- Gibbs, J.W., 1898, Nature, 59, 606
- Gravouil, A., Comberscure, A., 2001, IJNME, 50, 199
- Hirsch, C., 1997, "Numerical computation of internal and external flows", Wiley
- Ismail, F., Ken, Y.L., Othman, M., 2009, IJMA, 3, 239
- Ketcheson, D.I., Macdonald, C.B., Gottlieb, S., 2009, JANM, 59, 373
- King, A.R., Pringle, J.E., Livio, M., 2007, MNRAS, 376, 1740
- Lanzafame, G. 2008, PASJ, 60, 259
- Lanzafame, G., 2009, AN, 330, 843
- Lanzafame, G., 2010a, MNRAS, 408, 2336
- Lanzafame, G., 2010b, MNRAS, 408, 1551
- Lanzafame, G., 2010c, ASP, 429, 106
- Lanzafame, G., Belvedere, G., 2001, JKAS, 34, S313
- Lanzafame, G., Belvedere, G., 2002, PASJ, 54, 781
- Lanzafame, G., Belvedere, G., 2005, ApJ, 632, 499
- Lanzafame, G., Belvedere G., Molteni D., 1992, MNRAS, 258, 152

- Lanzafame, G., Belvedere G., Molteni, D., 2006, A&A, 453, 1027
- Lanzafame, G. Costa, V., Belvedere, G., 2011, ASP, in the press
- Lanzafame, G., Maravigna, F., Belvedere G., 2000, PASJ, 52, 515
- Lanzafame, G., Maravigna, F., Belvedere G., 2001, PASJ, 53, 139
- Lattanzio, J.C., Monaghan J.J., Pongracic, H., Schwarz, M.P., 1985, MNRAS, 215, 125
- LeVeque, R.J., 1992, "Numerical methods for conservation laws", Lectures in Mathematics, ETH Zürich, Birkhäuser
- LeVeque, R.J., 2002, "Finite volume methods for hiperbolic problems", Cambridge Univ. Press
- Lubow, S.H., Shu, F.H., 1975, MNRAS, 198, 383
- Majid, Z.A., Suleiman, M.B., Omar, Z., 2006, BMMSS, 29, 23
- Meglicki, Z., Wickramasinghe, D., Bicknell, G.V., 1993, MNRAS, 264, 691
- Miranda, I., Ferencz, R.M., Hughes, T.J.R., 1989, EESD, 18, 643
- Molteni, D., Belvedere, G., Lanzafame, G., 1991, MNRAS, 249, 748
- Monaghan, J.J., 1985, Comp. Phys. Rept., 3, 71
- Monaghan, J.J., 1992, ARA&A, 30, 543
- Monaghan, J.J., 1997, JCoPh, 136, 298
- Monaghan, J.J., Lattanzio, J.C., 1985, A&A, 149, 135
- Mosqueda, G., Ahmadizadeh, M., 2010, EESD, doi: 10.1002/eqe.1066
- Petkova, M., Springel, V., 2009, MNRAS, 396, 1383
- Press, W.H., Teukolsky, S.A., Vetterling, W.T., Flannery, B.P., 1992, "Numerical Recipes" (2nd ed.; Cambridge Univ. Press)
- Robert, A., 1969, "The integration of a spectral model of the atmosphere by the implicit method", Proc. of WMO/IUGG Symp. on NWP, Tokyo, Japan Metereological Agency, VII, 19-VII.24
- Robert, A. 1981, Atmos. Ocean., 19, 35
- Robert, A., Henderson, J., Turnbull, C., 1972, MWR, 100, 329
- Rook, R., Yildiz, M., Dost, S., 2007, Num. Heat Trans. B., 51, 1
- Sahin, M., Owens, R., 2003, IJNMF, 42, 57
- Sahin, M., Owens, R., 2003, IJNMF, 42, 79
- Shakura, N.I. 1972, Astron. Zh., 49, 921. (English tr.: 1973, Sov. Astron., 16, 756)
- Shakura, N.I., Sunyaev, R.A., 1973, A&A, 24, 337
- Susa, H., 2006, PASJ, 58, 445
- Staniforth, A., Côté, J., 1991, MWR, 119, 2206
- Toro, E.G., 1999, "Riemann solvers and numerical methods for fluid dynamics", Springer-Verlag
- Viau, S., Bastien, P., Cha, Seung-Hoon, 2006, ApJ, 639, 559
- Visbal, M.R., Gaitonde, D.V., 1999, AIAA, 10, 1231
- Whitehouse, S.C., Bate, M.R., 2004, MNRAS, 353, 1078
- Whitehurst, R., 1995, MNRAS, 277, 655
- Ying, W., Rose, D.J., Henriquez, C.S., 2008, IEEE Trans. on Biomed. Eng., 55, 2701

APPENDIX A: SPH AND PHYSICAL COHERENCE

As is well known, SPH formalism is technically based on the spatial distribution of the physical quantity $A(\mathbf{r})$, according to the interpolation integral (6), and its numerical counterpart (7). In such a conversion, the physical mass density of the i th SPH particle is either physically represented as $\rho_i = m_i n_i$, or numerically represented as $\rho_i = \sum_j \rho_j / n_j W_{ij} = \sum_j m_j W_{ij}$. Instead, the particle numerical density is either $n_i = \rho_i / m_i$, or $n_i = \sum_j W_{ij}$.

A necessary convergence is needed, because the two expressions for ρ_i or for n_i coincide only in the case of equal mass SPH particles, when $m_i = m_j$.

In addition, if we pay attention to the SPH particle masses, either $m_i = \rho_i / n_i$, or $m_i = \sum_j m_j / n_j W_{ij} = \sum_j \rho_j / n_j^2 W_{ij}$. These two expressions equal with each other only when $n_i = n_j$.

In some circumstances SPH particles could have different physical masses. In this case, the concept of SPH particle mass could be without any physical meaning whenever local densities are different: $\rho_i \neq \rho_j$.

To resolve such confusion, we modify the SPH formulation (7) according to one of these choices:

either

$$\begin{cases} m_i = \frac{\rho_i}{n_i} = \frac{1}{n_i} \sum_j \frac{\rho_j}{n_j} W_{ij} \\ n_i = \frac{\rho_i}{m_i} = \frac{1}{m_i} \sum_j \frac{\rho_j}{n_j} W_{ij} = \frac{1}{m_i} \sum_j m_j W_{ij} \\ \rho_i = m_i n_i = \sum_j m_j W_{ij}, \end{cases} \quad (\text{A1})$$

or

$$\begin{cases} m_i = \frac{\rho_i}{n_i} = \sum_j \frac{m_j}{n_j} W_{ij} = \sum_j \frac{\rho_j}{n_j^2} W_{ij} \\ n_i = \frac{\rho_i}{m_i} = \frac{1}{m_i} \sum_j \frac{m_j^2}{\rho_j} \frac{\rho_i}{m_i} W_{ij} = \frac{\rho_i}{m_i^2} \sum_j \frac{m_j^2}{\rho_j} W_{ij} \\ \rho_i = m_i n_i = n_i \sum_j \frac{m_j}{n_j} W_{ij}, \end{cases} \quad (\text{A2})$$

or

$$\begin{cases} m_i = \frac{\rho_i}{n_i} = \frac{\rho_i}{n_i} \sum_j \frac{1}{n_j} W_{ij} \\ n_i = \frac{\rho_i}{m_i} = \sum_j W_{ij} \\ \rho_i = m_i n_i = m_i \sum_j W_{ij}. \end{cases} \quad (\text{A3})$$

According to one of these choices, the full convergence between the SPH transformations and the full physical meaning of mass and densities are respected.